Electronic Supporting Information
Optical response of monolayer, few-layer and bulk tungsten disulfide

Maciej R. Molas,[1,*] Karol Nogajewski,[1,†] Artur O. Slobodeniuk,[1]
Johannes Binder,[1,2] Miroslav Bartos,[1] and Marek Potemski[1,2,‡]

[1] *Laboratoire National des Champs Magnétiques Intenses, CNRS-UGA-UPS-INSA-EMFL, 25, avenue des Martyrs, 38042 Grenoble, France*
[2] *Faculty of Physics, University of Warsaw, ul. Pasteura 5, 02-093 Warszawa, Poland*

I. INFLUENCE OF THE MONOLAYER PL ON THE EMISSION OF LIGHT FROM THICKER WS_2 FLAKES

It is worth to point out an important property of selected samples prepared by means of mechanical exfoliation, which may significantly affect their PL response. It particularly concerns the large-area flakes, which at the fabrication stage are subject to strongly non-uniform field of tearing force. Acting on thicker flakes, such force can locally split them into subunits composed of smaller number of layers, which nonetheless do not stop to interact with one another. For example, within a 3 ML-thick flake a pocket containing a 1 ML patch that is partially detached from its 2 ML-thick companion can be created. If optically probed, it may then give rise to the appearance of mixed PL signal comprising contributions of all three kinds, *i.e.* the 1 ML-, 2 ML-, and 3 ML-like, of course distorted by interactions between the two subunits. When performing preliminary measurements we experienced such a situation for some of our flakes composed of 3 MLs and 4 MLs, whose PL spectra were dominated by a set of prominent features resembling those observed for the monolayer. In order to avoid influencing our results by this artifact, we then carefully examined all flakes under consideration before qualifying them for further optical study.

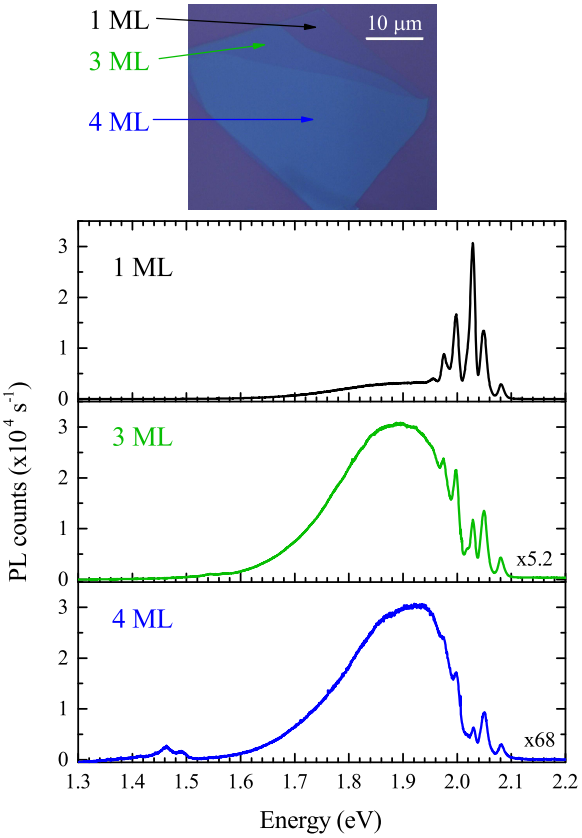

FIG. S1. PL spectra of the 1 ML-, 3 ML-, and 4 ML-thick flakes of WS_2, measured at T= 5 K and the excitation energy equal to 2.41 eV. The insets show the optical images of the studied flake.

II. THE BAND STRUCTURE OF S-TMD MULTILAYERS AT THE K POINTS OF THE BRILLOUIN ZONE

All the important features of multilayer S-TMDs exist also in a bilayer. Therefore we examine the latter system in details (following Ref. 1) and then generalise our consideration to the multilayer case. Finally we describe the properties of a bulk S-TMD.

A. Bilayer S-TMD.

We consider first the bilayer S-TMD as a system of two decoupled monolayers with 2H stacking order. In this case, the bilayer Bloch states at the $K^{\pm}$ point can be constructed from $K^{\pm}$ states of the lower and $K^{\mp}$ states of the upper layers respectively (see Fig. 12b).

Let us focus on the K^+ point of such system for clarity. Then, the conduction and valence band states of the lower layer can be written as $\{|d_0^{(1)}\rangle \otimes |\uparrow\rangle, |d_0^{(1)}\rangle \otimes |\downarrow\rangle\}$ and $\{|d_{+2}^{(1)}\rangle \otimes |\uparrow\rangle, |d_{+2}^{(1)}\rangle \otimes |\downarrow\rangle\}$. The superscript "(1)" denotes the "first" (lower) layer and $s = \uparrow, \downarrow$ marks the spin-up and spin-down states respectively. The symbols $d_{m=0,2}$ show from which transition metal atomic orbitals the quantum states are predominantly made. The conduction and valence band states of the upper layer are $\{|d_0^{(2)}\rangle \otimes |\uparrow\rangle, |d_0^{(2)}\rangle \otimes |\downarrow\rangle\}$, $\{|d_{-2}^{(2)}\rangle \otimes |\uparrow\rangle, |d_{-2}^{(2)}\rangle \otimes |\downarrow\rangle\}$. The superscript "(2)" denotes the "second" (upper) layer. The coordinate representation of the $|d_{+m}^{(1)}\rangle$ and $|d_{-m}^{(2)}\rangle$ states can be found in Ref. 2.

In the absence of interlayer hopping the valence and conduction bands at the K^+ point are doubly degenerated, and each pair $\{|d_{+m}^{(1)}\rangle \otimes |s\rangle, |d_{-m}^{(2)}\rangle \otimes |-s\rangle\}$ for fixed s and m is characterized by the same energy (see Fig. S2). $|-s\rangle$ represents the spin state with the opposite to s direction. In fact, the degeneracy is lifted by interlayer forces, which mix the basis states. The symmetry analysis[3] shows that only the valence band states with the same spin interact with each other. The conduction bands remain doubly degenerated.

Let us study the band structure of bilayer S-TMD quantitatively. We focus on the states at the K^+ point for tungsten-based compounds for brevity (the consideration of the opposite valley and/or molybdenum-based structures can be done by analogy).

The conduction band of bilayer contains two doubly degenerated subbands with the same splitting Δ_c as in monolayer. The sets of high- and low-energy states are $\{|d_0^{(1)}\rangle \otimes |\uparrow\rangle, |d_0^{(2)}\rangle \otimes |\downarrow\rangle\}$, $\{|d_0^{(1)}\rangle \otimes |\downarrow\rangle, |d_0^{(2)}\rangle \otimes |\uparrow\rangle\}$. The valence band states and their energies can be found from the Hamiltonian[1]

$$H_v(K^+) = \begin{bmatrix} \Delta_v/2 & t & 0 & 0 \\ t & -\Delta_v/2 & 0 & 0 \\ 0 & 0 & \Delta_v/2 & t \\ 0 & 0 & t & -\Delta_v/2 \end{bmatrix}, \tag{1}$$

written in the basis $\{|d_2^{(1)}\rangle \otimes |\uparrow\rangle, |d_{-2}^{(2)}\rangle \otimes |\uparrow\rangle, |d_{-2}^{(2)}\rangle \otimes |\downarrow\rangle, |d_2^{(1)}\rangle \otimes |\downarrow\rangle\}$. The diagonal matrix elements $\pm\Delta_v/2$ are the energies of corresponding states in the absence of interlayer hopping, which is defined by parameter t. According to block-diagonal form of Hamiltonian only the states with the same spin are mixed. Both blocks are equal and, therefore has the same spectrum. It results in two new doubly spin degenerated bands with energies $E_{\pm} = \pm\sqrt{\Delta_v^2/4 + t^2} \approx \pm(\Delta_v/2 + t^2/\Delta_v)$, see Fig.S2.

The highest energy E_+ valence bands states of bilayer are

$$|\Uparrow\rangle_+ = \{\cos\theta |d_2^{(1)}\rangle + \sin\theta |d_{-2}^{(2)}\rangle\} \otimes |\uparrow\rangle, \tag{2}$$

$$|\Downarrow\rangle_+ = \{\sin\theta |d_2^{(1)}\rangle + \cos\theta |d_{-2}^{(2)}\rangle\} \otimes |\downarrow\rangle, \tag{3}$$

where $\cos(2\theta) = \Delta_v/\sqrt{\Delta_v^2 + 4t^2}$. The low-energy E_- states can be calculated from E_+ ones by replacing $\cos\theta \to -\sin\theta, \sin\theta \to \cos\theta$.

The obtained structure of the conduction and valence bands helps us to find the properties of lowest energy optical transitions in bilayer S-TMD. There are four possible transitions of such type. Two of them have the energy $E_{X_A} - t^2/\Delta_v$ and intensities of lines

$$I_1^{\pm} = I_0 \cos^2\theta = I_0 \left(\frac{1}{2} + \frac{\Delta_v}{2\sqrt{\Delta_v^2 + 4t^2}}\right) \tag{4}$$

with $\sigma_{\pm}$ polarization of light. E_{X_A} and I_0 are the energy and intensity of A exciton transitions in monolayer (solid black arrow lines, which couple valence and conduction bands in left panel of Fig. S2). The second pair of transitions

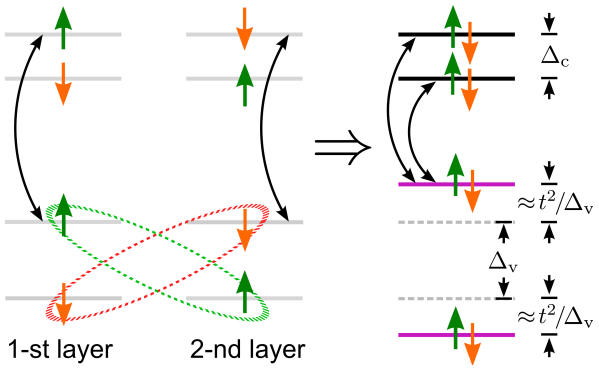

FIG. S2. (Left panel) Diagram of the bands position of two 2H-stacked S-TMD monolayers (at the K^+ point of the 1-st layer) in the absence of interlayer interaction. (Right part) Schematic drawing of the band positions in the bilayer, as a result of interaction between monolayers (presented by green and red dashed ellipses on the left panel). The green (orange) arrows indicate the spin-up (spin-down) subbands. Solid black arrow lines indicate the possible lowest energy optical transitions in both systems.

has the energy $E_{X_A} - \Delta_c - t^2/\Delta_v$ and intensity of lines

$$I_2^{\pm} = I_0 \sin^2\theta = I_0 \left(\frac{1}{2} - \frac{\Delta_v}{2\sqrt{\Delta_v^2 + 4t^2}} \right) \tag{5}$$

with $\sigma_\pm$ polarization of light. As one can see, the intensities of the left and right-polarized light in the case of bilayer are the same. Therefore, this material doesn't have the valley dependent optical dichroism as in monolayer S-TMD. This is due to the presence of the inversion symmetry in bilayer.

We estimate the energies and intensities of such transitions for the case of WS_2. For WS_2 $t = 0.0545$ eV, $\Delta_v = 0.421$ eV and $\cos\theta = 0.992$, $\sin\theta = 0.126$, see Ref. 1. Hence the exciton energy shift, due to mixing in valence band, is $t^2/\Delta_v \approx 7$ meV. The relative intensity $I_1^{\pm}/I_2^{\pm} \approx 60$. The same optical properties the bilayer has in the vicinity of K^- point.

B. Multilayer S-TMD.

A multilayer S-TMD crystal is a set of N monolayers, arranged in a pile with 2H stacking order. As in the bilayer case we enumerate all the S-TMD sheets from 1 to N, starting from the lowest (first) layer. Then, according to the 2H stacking all even layers are 180° rotated of the odd ones. Therefore the basis valence and conduction states at the K^+ point are $\{|d_{+2}^{(2m+1)}\rangle \otimes |\uparrow\rangle, |d_{+2}^{(2m+1)}\rangle \otimes |\downarrow\rangle\}$, $\{|d_{0}^{(2m+1)}\rangle \otimes |\uparrow\rangle, |d_{0}^{(2m+1)}\rangle \otimes |\downarrow\rangle\}$ for odd layers, and are $\{|d_{-2}^{(2m)}\rangle \otimes |\uparrow\rangle, |d_{-2}^{(2m)}\rangle \otimes |\downarrow\rangle\}$, $\{|d_{0}^{(2m)}\rangle \otimes |\uparrow\rangle, |d_{0}^{(2m)}\rangle \otimes |\downarrow\rangle\}$ for even ones, where $m = 1, 2, \ldots [N/2]$.

The interaction between layers is of the same type as in bilayer. Namely, the conduction bands do not interact, and as a result form spin-up and spin-down N degenerated conduction band states. The valence band states are mixed due to interlayer hopping. The corresponding valence band Hamiltonian is $2N \times 2N$ block-diagonal matrix. Each $N \times N$ block acts on spin-up and spin-down states separately. The eigenvalues of the matrix defines the positions of new valence bands.

Note that $N = 2M$ (even) and $N = 2M + 1$ (odd) multilayers have different properties from spectroscopic point of view.[4] For $N = 2M$ (*i.e.* 2 MLs, 4 MLs, 6 MLs,...), system possesses the inversion symmetry. Therefore, valley dependent physical properties of each monolayer, such as optical selection rules, are averaging to zero in such systems. It reflects also in the fact that for even number of layers all the new valence bands are, as minimum, doubly spin degenerated.

For $N = 2M + 1$ (*i.e.* 3 MLs, 5 MLs, 7 MLs,...), there is one non-compensated additional layer in the crystal. It results in valley dependent optical dichroism in the system. However, it is suppressed by the large number of layers. The spectrum of such system contains the set of M doubly spin degenerated levels (very close by the structure to 2M multilayer) and two additional levels with energies $\pm\Delta_v/2$.

The optical intensities of excitonic transitions in multilayers can be found by solving the eigenvalue problem for $N \times N$ matrices, mentioned above. They are presented in Fig. S3.

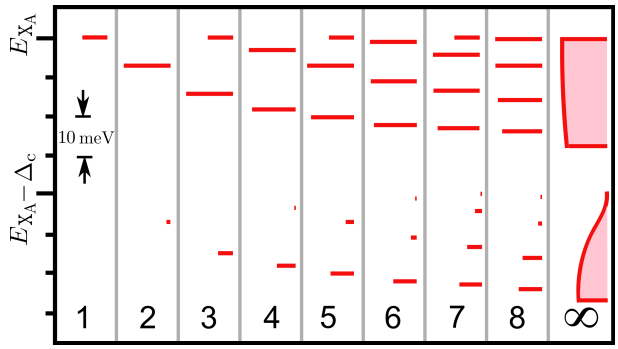

FIG. S3. The position and relative intensities of lowest energy transitions in multilayer WS_2, as a function of number of layers. The length of each line from the top part of the picture is proportional to the intensity of corresponding transition. The intensity of transitions, which correspond to the bottom set of lines, is 10 times smaller than presented on the picture.

The difference between odd and even multilayers disappears in the limit $N \to \infty$. Therefore, it is convenient to consider the bulk S-TMD as the even layered system $N = 2M$. Corresponding calculations are done in the next subsection.

C. The band structure of bulk S-TMD.

For a bulk S-TMD, according to previous consideration, there is no interlayer hopping for conduction states in vicinity of $K^{\pm}$ points, that reflects in spin-up and spin-down N degenerated conduction bands. The valence band states interact with each other and form new bands. In the bulk case $M \to \infty$ all these new states belong to one wide band, which has the meaning of the band in out-of-plane (z) direction. Below we obtain this conclusion quantitatively.

The bulk S-TMD with $N = 2M$ layers can be presented as a pile of M bilayers. The length of periodicity in such system coincides with the lattice constant c of the bulk in out-of-plane (z) direction. Therefore we slice the bulk on the elementary blocks with two layers inside, and then study the hopping between these blocks. In further, we focus on the states at the K^+ point in details (the case of K^- is described in the analogous way).

Let us consider the m-th bloc of sliced system, mentioned above (see Fig.S4). Its valence bands basis functions are $\{|d_2^{(m)}\rangle \otimes |\uparrow\rangle, |d_2^{(m)}\rangle \otimes |\downarrow\rangle, |d_{-2}^{(m)}\rangle \otimes |\uparrow\rangle, |d_{-2}^{(m)}\rangle \otimes |\downarrow\rangle\}$. The each state in the system we present as

$$|\Uparrow\rangle = \frac{1}{\sqrt{M}} \sum_{m=1}^{M} \{\Psi_m^{\uparrow} |d_2^{(m)}\rangle + \Phi_m^{\uparrow} |d_{-2}^{(m)}\rangle\} \otimes |\uparrow\rangle, \tag{6}$$

$$|\Downarrow\rangle = \frac{1}{\sqrt{M}} \sum_{m=1}^{M} \{\Psi_m^{\downarrow} |d_{-2}^{(m)}\rangle + \Phi_m^{\downarrow} |d_2^{(m)}\rangle\} \otimes |\downarrow\rangle. \tag{7}$$

The variables Ψ_m^s and Φ_m^s correspond to high and low-energy excitations of valence band. The eigenvalue problem in this representation takes the form

$$E\Psi_m^{\uparrow} = \frac{\Delta_v}{2}\Psi_m^{\uparrow} + t\Phi_m^{\uparrow} + t\Phi_{m-1}^{\uparrow}, \tag{8}$$

$$E\Psi_m^{\downarrow} = \frac{\Delta_v}{2}\Psi_m^{\downarrow} + t\Phi_m^{\downarrow} + t\Phi_{m+1}^{\downarrow}, \tag{9}$$

$$E\Phi_m^{\downarrow} = -\frac{\Delta_v}{2}\Phi_m^{\downarrow} + t\Psi_m^{\downarrow} + t\Psi_{m-1}^{\downarrow}, \tag{10}$$

$$E\Phi_m^{\uparrow} = -\frac{\Delta_v}{2}\Phi_m^{\uparrow} + t\Psi_m^{\uparrow} + t\Psi_{m+1}^{\uparrow}. \tag{11}$$

The schematic representation of these relations is shown in Fig. S4

Introducing the substitution

$$\begin{bmatrix} \Psi_m^s \\ \Phi_m^s \end{bmatrix} = e^{ikcm} \begin{bmatrix} \Psi_k^s \\ \Phi_k^s \end{bmatrix} \tag{12}$$

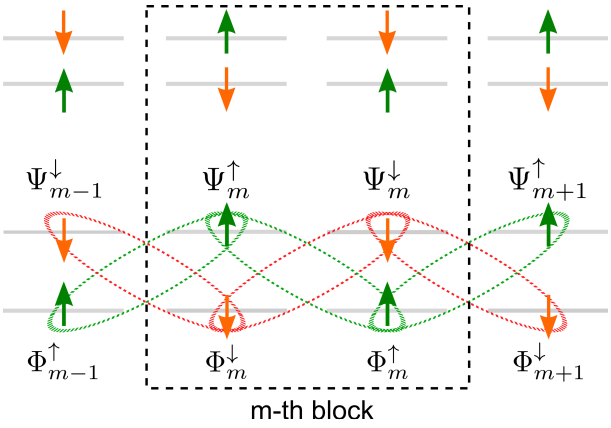

FIG. S4. Schematic representation of the interaction between the states of m-th block and its neighbours at the K^+ point of multilayer S-TMD. The interactions are denoted by green and red dashed ellipses. The green (orange) arrows indicate the spin-up (spin-down) subbands in the conduction and valence bands.

and periodic boundary conditions $k \in k_n = 2\pi n/c\mathrm{M}, n \in (-[\mathrm{M}/2], [\mathrm{M}/2]]$, one present the relations between new states in the form

$$E(k)\begin{bmatrix}\Psi^{\uparrow}_{k}\\ \Phi^{\uparrow}_{k}\end{bmatrix} = \begin{bmatrix}\Delta_{\mathrm{v}}/2 & 2te^{-i\frac{kc}{2}}\cos(\frac{kc}{2})\\ 2te^{i\frac{kc}{2}}\cos(\frac{kc}{2}) & -\Delta_{\mathrm{v}}/2\end{bmatrix}\begin{bmatrix}\Psi^{\uparrow}_{k}\\ \Phi^{\uparrow}_{k}\end{bmatrix} \tag{13}$$

$$E(k)\begin{bmatrix}\Psi^{\downarrow}_{k}\\ \Phi^{\downarrow}_{k}\end{bmatrix} = \begin{bmatrix}\Delta_{\mathrm{v}}/2 & 2te^{i\frac{kc}{2}}\cos(\frac{kc}{2})\\ 2te^{-i\frac{kc}{2}}\cos(\frac{kc}{2}) & -\Delta_{\mathrm{v}}/2\end{bmatrix}\begin{bmatrix}\Psi^{\downarrow}_{k}\\ \Phi^{\downarrow}_{k}\end{bmatrix} \tag{14}$$

The spin-up and spin-down states are decoupled in this case, but they have the same energy spectrum $E(k) = \pm\sqrt{\Delta_{\mathrm{v}}^2/4 + 4t^2\cos^2(kc/2)}$. This fact reflects that all new valence bands of the bulk are doubly spin-degenerated. The corresponding band structure, in the limit $\mathrm{M}\to\infty$ ($k_n \to k_z$) is presented in Fig. S5.

Let us consider the higher energy bands $E(k_z) \geq \Delta_{\mathrm{v}}/2$ more precisely. The corresponding eigenstates are

$$\begin{bmatrix}\Psi^{\uparrow}_{k_z}\\ \Phi^{\uparrow}_{k_z}\end{bmatrix} = \begin{bmatrix}\cos\theta_{k_z}\\ e^{i\frac{k_z c}{2}}\sin\theta_{k_z}\end{bmatrix}, \quad \begin{bmatrix}\Psi^{\downarrow}_{k_z}\\ \Phi^{\downarrow}_{k_z}\end{bmatrix} = \begin{bmatrix}\cos\theta_{k_z}\\ e^{-i\frac{k_z c}{2}}\sin\theta_{k_z}\end{bmatrix}, \tag{15}$$

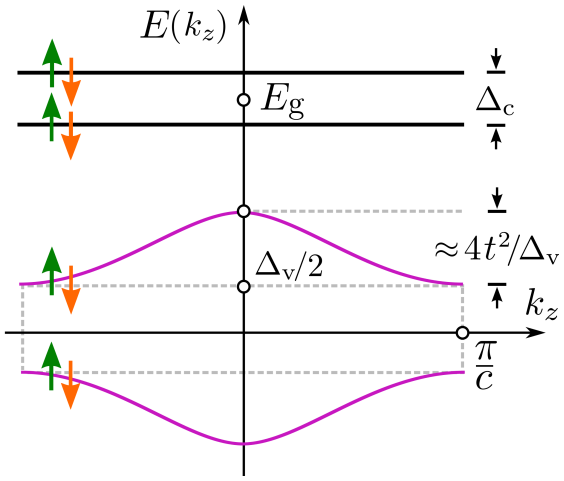

FIG. S5. The valence (purple lines) and conduction (black lines) energy bands as a function of out-of-plane wave-vector k_z at the K^+ point. E_g represents the position of band gap in monolayer S-TMD. The green (orange) arrows indicate the spin-up (spin-down) subbands in the conduction and valence bands.

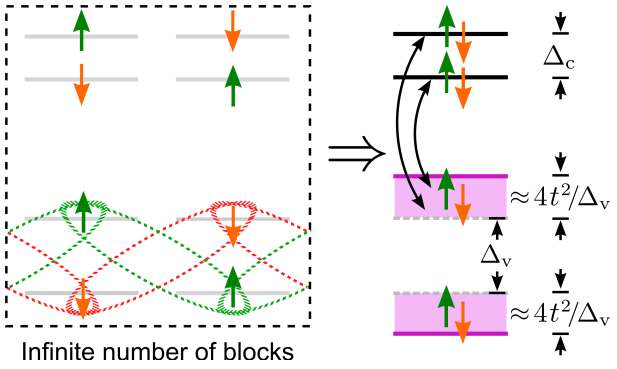

FIG. S6. (Left panel) Diagram of the conduction and valence bands position in one of the infinite blocks, which form the bulk S-TMD. The green and red dashed ellipses represent the interaction between the states inside the block and its neighborhoods. (Right panel) The band structure of the bulk at the K^+ point. Each horizontal line inside the purple rectangular corresponds to the state with $k_z \in [-\pi/c, \pi/c]$. The possible, lowest energy, optical transitions are presented by black solid arrow lines. The green (orange) arrows indicate the spin-up (spin-down) subbands in the conduction and valence bands.

where we introduced the notation

$$\cos(2\theta_{k_z}) = \frac{\Delta_v}{\sqrt{\Delta_v^2 + 16t^2\cos^2(k_z c/2)}} = \frac{\Delta_v}{2E(k_z)} \tag{16}$$

As a result, the eigenstates of the bulk have the form

$$|\Uparrow\rangle_{k_z} = \frac{1}{\sqrt{M}}\sum_{m=1}^{M} e^{ik_z cm}\{\Psi^{\uparrow}_{k_z}|d_2^{(m)}\rangle + \Phi^{\uparrow}_{k_z}|d_{-2}^{(m)}\rangle\}\otimes|\uparrow\rangle, \tag{17}$$

$$|\Downarrow\rangle_{k_z} = \frac{1}{\sqrt{M}}\sum_{m=1}^{M} e^{ik_z cm}\{\Psi^{\downarrow}_{k_z}|d_{-2}^{(m)}\rangle + \Phi^{\downarrow}_{k_z}|d_2^{(m)}\rangle\}\otimes|\downarrow\rangle. \tag{18}$$

They correspond to spin-up and spin-down valence band states with non-zero momentum k_z. The structure of these functions defines the optical properties of the bulk. Indeed, there are two subset of optical transitions from wide valence zone (presented by the purple rectangular in Fig. S6) to spin-up and spin-down conduction band states (presented by two straight black lines). The first set of transitions has the energies $E_{X_A} - E(k_z)$ with intensities

$$I^s_{k_z} = I_0|\Psi^s_{k_z}|^2 = I_0\left(\frac{1}{2} + \frac{\Delta_v}{4E(k_z)}\right). \tag{19}$$

The second set of transitions has the energies $E_{X_A} - \Delta_c - E(k_z)$ with intensities

$$I^s_{k_z} = I_0|\Phi^s_{k_z}|^2 = I_0\left(\frac{1}{2} - \frac{\Delta_v}{4E(k_z)}\right). \tag{20}$$

Due to this result, the transitions between spin-up and spin-down states have the same intensity. It reflects the absence of valley dependent circular dichroism in such system. Moreover, the total amount of light which is absorbed by material is not changed, but is only redistributed between the new bands.

The obtained result helps us to estimate the effective valence band mass m_z in z direction. Expanding the square root at small momenta k_z for high energy valence band at the K^+ point, we obtain $m_z = \hbar^2\Delta_v/2t^2c^2$. Substituting the previous parameters for WS_2 and taking $c = 12.32$Å[5] one gets $m_z \approx 3.6m_0$, where m_0 is free-electron mass. Therefore the whole dispersion of the valence band of the bulk S-TMD in K^+ point can be written as

$$E_{\pm}(\mathbf{k}, k_z) = \pm\frac{\Delta_v}{2} \pm \frac{4t^2}{\Delta_v} - \frac{\hbar^2\mathbf{k}^2}{2m_{\pm}} \mp \frac{\hbar^2 k_z^2}{2m_z}, \tag{21}$$

where $\mathbf{k} = (k_x, k_y)$ are in-plane wave-vector of valence electrons. $E_{\pm}(\mathbf{k}, k_z)$ represent the energy dispersion of higher and lower valence bands of the bulk, and $m_{\pm}$ are the effective masses of the higher and lower energy valence bands in monolayer.

III. AMBIGUOUS FITTING OF THE REFLECTANCE CONTRAST SPECTRUM OF BILAYER WS_2

Fitting the reflectance contrast spectrum of bilayer WS_2 with a model curve calculated within the framework of transfer-matrix method gives an ambiguous answer to the question how many (one or two) Lorentzian-type resonances one should take into account to correctly reproduce the shape of the A-exciton feature. Solving this issue would greatly help to establish the significance of intra- and interlayer excitonic transitions described in the previous section for the absorption of light in WS_2 multilayers. Unfortunately, as shown in Fig. S7, the difference between the fits obtained for one (Fig. S7(a)) and two (Fig. S7(b)) resonance contributions to the dielectric function of bilayer WS_2 in the vicinity of 2.05 eV is in our case purely quantitative. On a qualitative level, given the linewidths of the excitonic transitions involved which are as large as 35 meV, both of them equally well reproduce the experimental spectrum. It means that in order to ultimately determine the single- or double-resonance character of the A-exciton feature in the absorption-like response of bilayer WS_2 one has to consider higher-quality samples with narrower excitonic transitions. As recently demonstrated for monolayers of MoS_2 (Ref. 6) and WSe_2 (Ref. 7), such structures can be fabricated by encapsulating the central S-TMD flake with two flakes of hexagonal boron nitride. If the reported reduction of linewidth of excitonic transitions in such samples by more than one order of magnitude with respect to the non-encapsulated ones would also hold for bilayer WS_2, the shape of its reflectance contrast spectrum should leave no doubt about the number of resonances contributing to the A-exction feature.

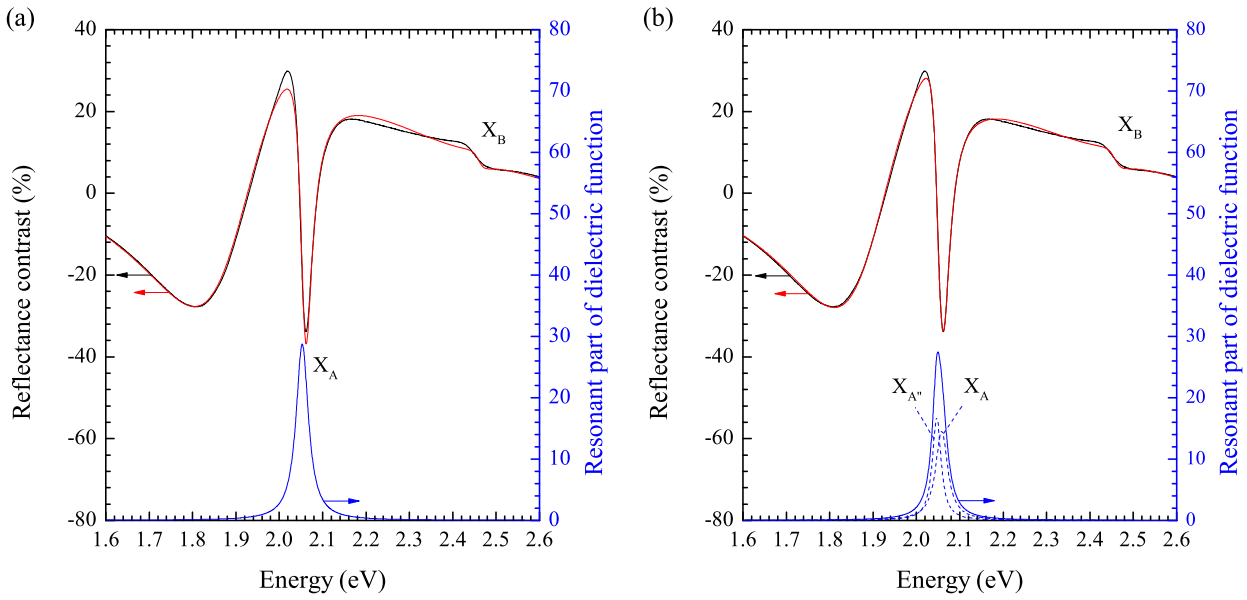

FIG. S7. Comparison between fits (red curves) to the reflectance contrast spectrum (black curves) of bilayer WS_2 obtained within the framework of transfer-matrix method when assuming that the A-exciton feature in the vicinity of 2.05 eV originates from (a) single excitonic resonance (X_A) and (b) two closely spaced excitonic resonances denoted by X_A and $X_{A"}$. X_B stands for the B-exciton resonance. Drawn in blue are corresponding Lorentzian-type contributions to the imaginary part of dielectric function of bilayer WS_2 (the one associated with the B exciton is purposely not shown in the graphs).

IV. SIMULATED REFLECTANCE CONTRAST SPECTRA FOR OPTICAL TRANSITIONS DUE TO INTRALAYER EXCITONS IN WS_2 MULTILAYERS

It is already well established that the optical response of structures composed of thin flakes of S-TMD materials exfoliated onto alien substrates, like a piece of Si/SiO_2 wafer, is strongly affected by interference effects.[8] Because of this fact, predicting the shape of a reflectance contrast spectrum for a set of given excitonic transitions without taking into account the internal structure of a dielectric stack under consideration represents a difficult task which may often lead to confusing and/or incorrect conclusions. It particularly applies to the intra- and interlayer excitonic transitions in WS_2 multilayers discussed in Sec. II and depicted in Fig. S3. In order to see the final shape of reflectance contrast spectra of different WS_2 N-layers supported by $Si/(320\,nm)\,SiO_2$ substrate, which are determined by these transitions, we first evaluated their contribution to the imaginary part of dielectric function of according WS_2 layers by implementing them into the Lorentz-oscillator model with a broadening of every individual transition equal to 20 meV (in agreement with our experimental data). While doing so we assumed that $E_{X_A} = 2.056$ eV and considered only the intralayer transitions (the upper branch of lines in Fig. S3) since the interlayer ones (the lower branch of lines in Fig. S3) with their intensities being smaller by one to two orders of magnitude than those of the intralayer transitions would have negligible impact on the resultant reflectance contrast spectra. The results of such calculations performed for WS_2 layers composed of 2 to 8 MLs are presented in Fig. S8(a). In the next step, by making use of the transfer-matrix method, we simulated on their basis the corresponding reflectance contrast spectra displayed in Fig. S8(b). As one can see, they surprisingly well reproduce the shape and general evolution of the experimental traces shown in Fig. 11 of the main text (a small blue-shift of the feature appearing in the vicinity of 2.05 eV with increasing the number of layers may results from neglecting in our calculations the Coulomb interactions and/or the band-gap renormalization). Given the simplicity of our single-particle considerations this is quite a remarkable finding. Nevertheless, a much more detailed and accurate theory is required to confirm whether the peculiar fine structure of the A-exction line in the reflectance contrast spectra of WS_2 multilayers indeed originates from the intralayer excitonic transitions as discussed in Sec. II.

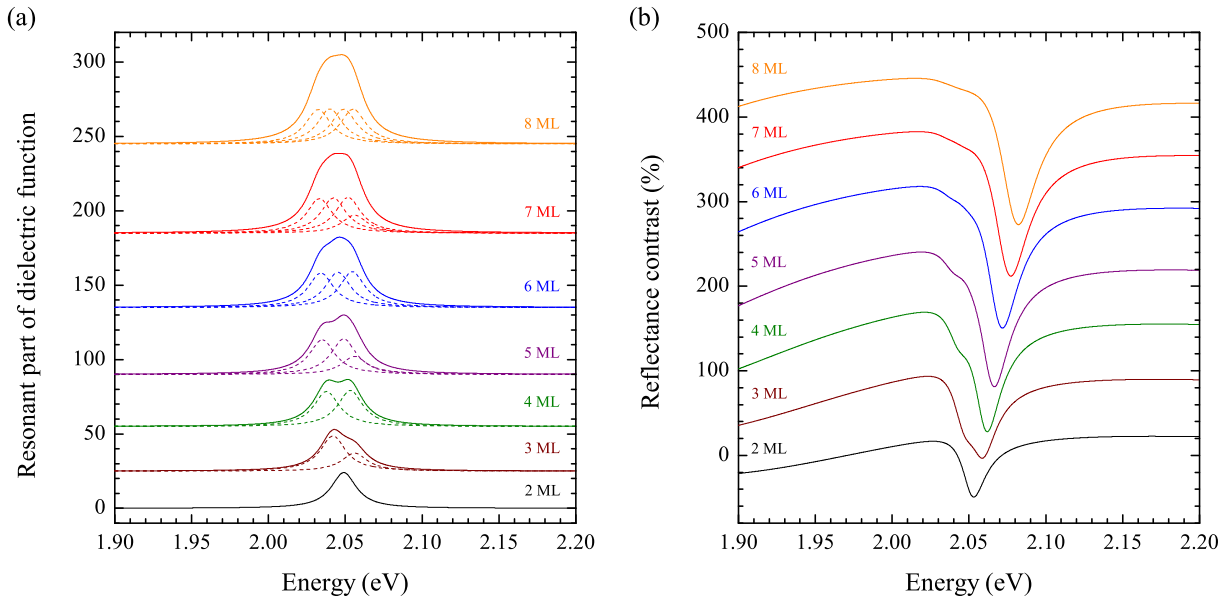

FIG. S8. (a) Resonant contributions to the imaginary part of dielectric function of WS_2 multilayers and (b) corresponding reflectance contrast spectra calculated on the basis of intralayer excitonic transitions discussed in Sec. II and shown in Fig. S3. Drawn with dashed lines in panel (a) are individual transitions, each one with an assumed broadening of 20 meV as deduced from our experimental data.

V. FUNDAMENTAL EXCITONIC RESONANCES AS A FUNCTION OF TEMPERATURE

Aiming at learning more about the properties of excitonic resonances associated with the transitions in the vicinity of the A exciton, we measured the RC spectra of the 1 ML-, 2 ML-, and 3 ML-thick flakes as well as of the bulk flake of 32 nm thickness as a function of temperature, see Fig. S9. For few-layer flakes, the temperature evolutions of the X_A and $X_{A"}$ transitions could be followed in the whole temperature range, whereas for the bulk flake, due to generally small changes in the RC signal even for the most pronounced features, we were not able to reliably extract the contribution coming from the $X_{A"}$ features at temperatures higher than 180 K.

Concerning other features, the T_2 transition, which is clearly visible in the RC spectrum of the 1 ML at 5 K - see Fig. S9(a), quickly disappears from experimental traces around 40 K, which makes the analysis of its temperature evolution idle. It is not the case of an excited excitonic transition denoted by X_{A*}, which survives in the RC spectra

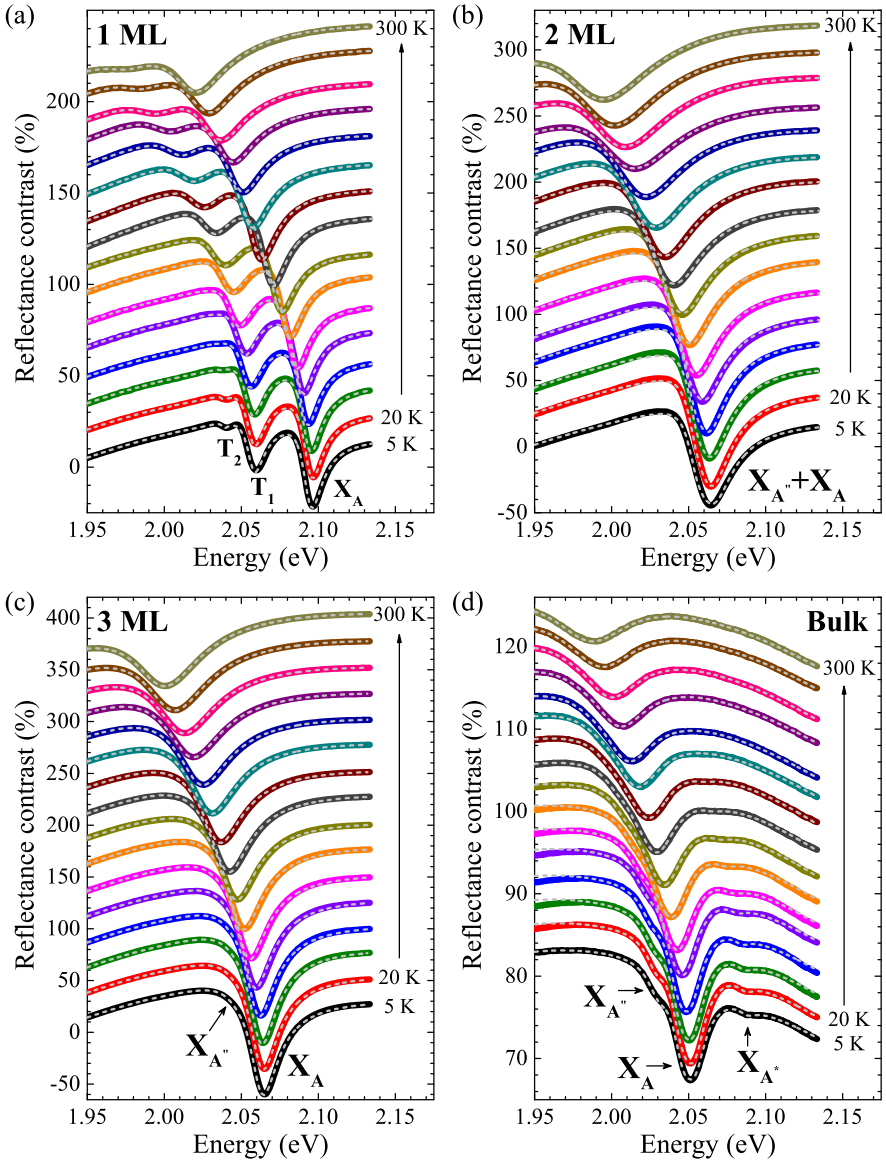

FIG. S9. RC spectra of (a) 2 ML-, (b) 3 ML-, and of the bulk flake of 32 nm thickness, measured for different temperatures ranging from 5 K up to 300 K. The dashed grey lines are the corresponding modelled curves. The spectra are vertically shifted for clarity purpose.

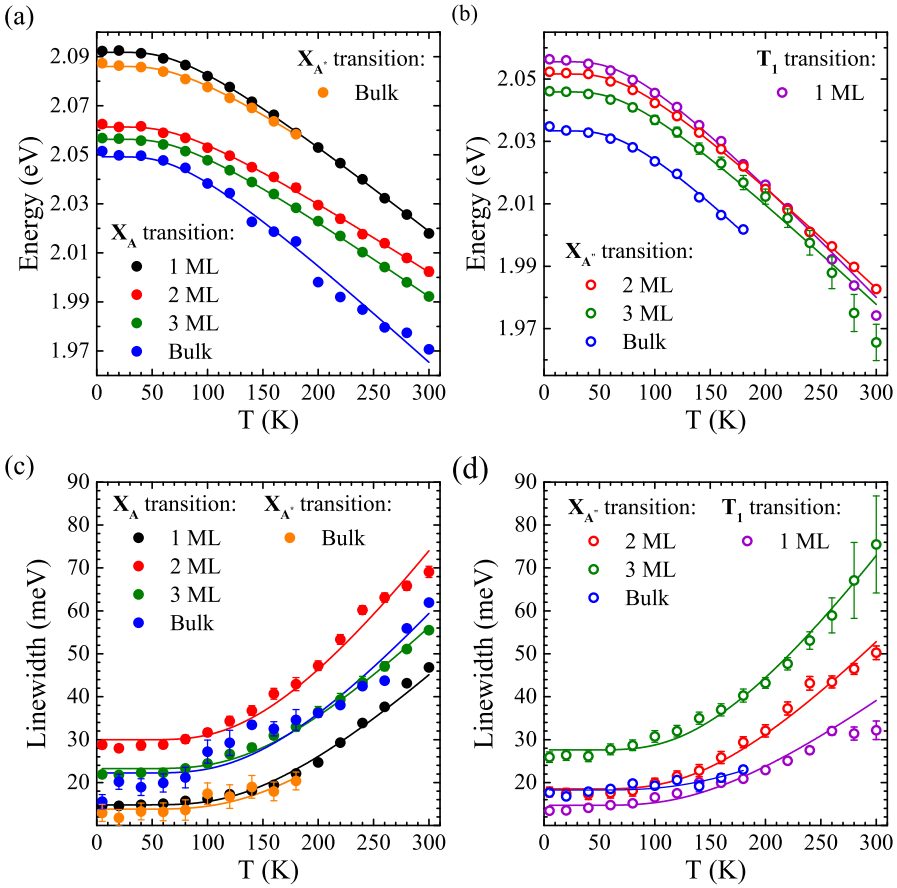

FIG. S10. Temperature evolution of the: (a) energy and (c) linewidth of the X_A andX_{A^*} transitions; (b) energy and (d) linewidth of the T_1 and X_{A^*} transitions extracted from the RC spectra measured on the 1 ML-, 2 ML-, and 3 ML-thick flakes, as well as on the bulk flake of 32 nm thickness. The solid circles represent the experimental results while the solid curves are fits to the data obtained with the aid of Eq. 23 and 24.

of the bulk flake up to ∼180 K, and as such can be reliably fitted with a model dependence. For all traces presented in Fig. S9, the energies of all excitonic resonances experience a red shift as the temperature is being increased from 5 K up to 300 K. This type of evolution, which is characteristic of many semiconductors, can be reproduced with the aid of formulae proposed by Varshni[9] and O'Donnell *et al.*,[10] both describing the temperature dependence of the energy gap. The Varshni relation is given by:

$$E_g(T) = E_0 - (\alpha T^2)/(T + \beta), \tag{22}$$

where E_0 stands for the band gap at absolute zero temperature, while α and β represent the fitting parameters related to the electron(exciton)-phonon interaction and Debye temperature (T_D), respectively. From the fact that the used relation describes the temperature evolution of the band gap, it correctly reproduces also the energies of fundamental excitonic resonances, we conclude that binding energies of excitons they correspond to do not depend on temperature.

The results of fitting our experimental data shown in Figs. S10(a) and S10(b) with the Varshni relation are summarized in the first row of Tab. I. We noticed that allowing both α and β parameters to be varied at the same time led to a whole family of curves, which closely followed the experimental points but lacked the physical sense. This observation pushed us towards fixing the Debye temperature at the same level for all the flakes considered. Based on the quality of resulting fittings, we assumed that β =220 K, not far from the value reported for bulk WS_2 in Ref. 11. In order to justify our decision, let us recall that for $T > T_D$ the majority phonons that can be excited

TABLE I. Parameters of fitting the temperature dependence of the resonance energy with Varshni and O'Donnell relations, and of the lineshape broadening with the Rudin relation, obtained for X_A, X_{A^*}, $X_{A"}$ and T_1 transitions for 1 ML, 2 ML, and 3 ML flakes and the bulk flake of 32 nm thickness.

	T_1	$X_{A"}$			X_A				X_{A^*}
Parameter	1 ML	2 ML	3 ML	bulk	1 ML	2 ML	3 ML	bulk	bulk
Varshni's relation									
E_0 (eV)	2.058	2.054	2.050	2.036	2.094	2.063	2.059	2.053	2.088
α (10^{-4} eV/K)	4.32	4.09	4.48	4.17	4.31	3.52	3.83	5.02	3.56
O'Donnell's relation									
E_0 (eV)	2.056	2.051	2.046	2.033	2.092	2.061	2.056	2.049	2.086
S	2.20	2.01	1.99	2.15	2.13	1.73	1.87	2.45	1.83
Rudin's relation									
γ_0 (meV)	15	19	23	18	15	30	28	22	14
γ' (meV)	115	161	154	79	142	207	212	174	126

in a crystal are those with wave vectors close to the BZ boundaries. On the other hand, at low temperatures ($T \ll T_D$), the only phonons that play an important role are those related to the centre of the BZ.[12] One may say that T_D sets the lower bound for the temperature range, in which practically all possible phonon modes of a given system can be in principle observed. The number and symmetry of these modes are specified by the crystal structure, which in the case of TMDC materials does not significantly change with the layer thickness. This means that there is no reason to expect T_D to be different for flakes composed of different number of layers. Concerning the value of T_D, as room-temperature measurements usually resolve a complete phonon spectrum of both conventional semiconductors and TMDCs, it should not be substantially larger than 300 K. Taking all these remarks into account, our choice of β =220 K dictated by the quality of fitting the experimental data with the Varshni relation seems to be a reasonable estimation. For fixed β it can be noticed that the parameter α obtained for flakes of different thicknesses exhibits a larger variance for the A" transition than for the neutral excitonic resonance.

The relation proposed by O'Donnell *et al.*[10] describes the temperature dependence of the band gap in terms of an average phonon energy $<\hbar\omega>$ and reads:

$$E_g(T) = E_0 - S <\hbar\omega> [\coth(<\hbar\omega>/2k_BT) - 1], \tag{23}$$

where S is the coupling constant and k_B denotes the Boltzmann constant. We found that $<\hbar\omega>$ stayed on nearly the same level, ∼20 meV, for all the flakes under study. As a consequence, similarly to the parameter β discussed above, we kept it fixed during the final run of our data analysis.

The results of fitting the experimental points with O'Donnell's relation are displayed in Figs S10(a) and S10(b) in the form of solid curves described by the set of parameters summarized in the second row of Tab. I. As can be seen, in analogy with the parameter α from Varshni's equation, the variance of the parameter S obtained for flakes composed of different number of layers is larger for the T_1 and $X_{A"}$ features than for the X_A excitonic resonance. In spite of this similarity, it turned out that the O'Donnell relation gives significantly better fits to our data as compared to what we were able to get with the aid of Varshni's formula.

Panels (c) and (d) of Fig. S10 present the temperature evolution of the linewidth of the studied resonances, respectively. In semiconductors, such an evolution can be described by so-called Rudin's relation[13] which is given by:

$$\gamma(T) = \gamma_0 + \sigma T + \gamma' \frac{1}{(\exp^{\hbar\omega/kT} - 1)}, \tag{24}$$

where γ_0 denotes the broadening of a given spectral line at 0 K, the term linear in temperature (σ) quantifies the interaction of excitons with acoustic phonons (of negligible meaning for the present work), γ' arises from the interaction of excitons with LO phonons, and $\hbar\omega$ is the LO phonon energy, which was taken to be equal to 45 meV, due to the highest density of states.[14] Note that this value corresponds to the LO phonon energy found in an analogous experiment done on bulk WS_2.[11]

The results of fitting our experimental points with Rudin's relation are presented in Figs S10(c) and S10(d) as solid curves described by the set of parameters shown in the third row of Tab. I. Due to different vertical offsets determined by γ_0, which effectively counterbalance the slopes of particular traces, they all look essentially the same concerning the rate at which the broadenings of excitonic resonances develop with increasing the temperature. One can also notice that, irrespective of the flake thickness, the values of γ' obtained for the X_A exciton are larger than those established for the T_1 and X_{A^-} features, which indicates that phonon-assisted scattering of the former complexes is more efficient. Furthermore, in agreement with conclusions drawn in Ref. 15 for WSe_2 and in Ref. 16 for $MoSe_2$, we see a pronounced increase in γ' between the monolayer and the bilayer for the A exciton.

* maciej.molas@gmail.com
† karol.nogajewski@lncmi.cnrs.fr
‡ marek.potemski@lncmi.cnrs.fr

[1] Z. Gong, G.-B. Liu, H. Yu, D. Xiao, X. Cui, X. Xu, and W. Yao, Nature Communications **4**, 2053 (2013).
[2] A. M. Jones, H. Yu, J. S. Ross, P. Klement, J. Ghimire, Nirmal J.and Yan, D. G. Mandrus, W. Yao, and X. Xu, Nat. Phys. **10**, 130 (2014).
[3] G.-B. Liu, D. Xiao, Y. Yao, X. Xu, and W. Yao, Chem. Soc. Rev. **44**, 2643 (2015).
[4] H. Zeng, G.-B. Liu, J. Dai, Y. Yan, B. Zhu, R. He, L. Xie, S. Xu, X. Chen, W. Yao, and X. Cui, Sci. Rep. **3**, 1608 (2013).
[5] W. Schutte, J. D. Boer, and F. Jellinek, J. Solid State Chem. **70**, 207 (1987).
[6] F. Cadiz, E. Courtade, C. Robert, G. Wang, Y. Shen, H. Cai, T. Taniguchi, K. Watanabe, H. Carrere, D. Lagarde, M. Manca, T. Amand, P. Renucci, S. Tongay, X. Marie, and B. Urbaszek, Phys. Rev. X **7**, 021026 (2017).
[7] M. Manca, M. M. Glazov, C. Robert, F. Cadiz, T. Taniguchi, K. Watanabe, E. Courtade, T. Amand, P. Renucci, X. Marie, G. Wang, and B. Urbaszek, Nat. Commun. **8**, 14927 (2017).
[8] D.-H. Lien, J. S. Kang, M. Amani, K. Chen, M. Tosun, H.-P. Wang, T. Roy, M. S. Eggleston, M. C. Wu, M. Dubey, S.-C. Lee, J.-H. He, and A. Javey, Nano. Lett. **15**, 1356 (2015).
[9] Y. Varshni, Physica **34**, 149 (1967).
[10] K. P. O'Donnell and X. Chen, Appl. Phys. Lett. **58**, 2924 (1991).
[11] D. Dumcenco, H. Hsu, Y. Huang, C. Liang, K. Tiong, and C. Du, Mater. Chem. Phys. **111**, 475 (2008).
[12] B. N. Roy, John Wiley & Sons Ltd., Great Britain (2002).
[13] S. Rudin, T. L. Reinecke, and B. Segall, Phys. Rev. B **42**, 11218 (1990).
[14] A. Molina-Sánchez and L. Wirtz, Phys. Rev. B **84**, 155413 (2011).
[15] A. Arora, M. Koperski, K. Nogajewski, J. Marcus, C. Faugeras, and M. Potemski, Nanoscale **7**, 10421 (2015).
[16] A. Arora, K. Nogajewski, M. Molas, M. Koperski, and M. Potemski, Nanoscale **7**, 20769 (2015).